V International Conference on Particle-based Methods – Fundamentals and Applications
PARTICLES 2017
P. Wriggers, M. Bischoff, E. Oñate, D.R.J. Owen, & T. Zohdi (Eds)

INCLINED CHUTE FLOW OF ROD-LIKE PARTICLES USING THE DISCRETE ELEMENT METHOD

MASATO SAEKI [1] AND RYOHEI ARAI [2]

[1] Dept. of Mechanical Engineering, Fuculty of Engineering,
Shibaura Institute of Technology
3-7-5 Toyosu, Koto-ku, Tokyo 135-8548, Japan
E-mail: saeki@sic. shibaura-it.ac.jp
URL: http://www.sic.shibaura-it.ac.jp/~saeki/index_E.html

[2] Graduate school Engineering and Science, Shibaura Institute of Technology,
3-7-5 Toyosu, Koto-ku, Tokyo 135-8548, Japan
E-mail: md14004@shibaura-it.ac.jp

Key words: Granular Materials, DEM, Rod-like particles, Contact Problems.

Abstract. An inclined chute flow of rod-like particles is investigated both experimentally and analytically. The behavior of the particles is solved by the discrete element method (DEM). The rod-like particle model consists of a cylinder, capped at both ends by hemispheres whose radii are the same as the radius of the cylinder. The rod-like particles have three translational degrees of freedom, their rotational motion being described through quaternions, and the interparticle contact is described by a force that accounts for the elastic and dissipative interactions. The contact patterns for the rod-like particles are classified into six types. In the experiment, brass and acrylic resin cylinders of uniform size were used. The validity of the theory was confirmed by comparing the experimental and analytical results. In addition, the effect of the particle material on the flow pattern was examined.

1 INTRODUCTION

The discrete element method (DEM) has become established as the primary numerical technique for simulating many industrial granular flows. The main advantage of the DEM is that it makes it possible to consider the effect of granularity, such as the particle size, number of particles, and friction between two particles. It is known that the dynamics of granular materials are strongly affected by their shape. When examining the effect of the particle shape on granularity, rod-like particles are often used. This is because rod-like particles are widely used in chemical, pharmaceutical, and other industries [1, 2]. There is considerable descriptive detail available on the dynamics of rod-like particles. However, most previous theoretical analyses have focused on the multi sphere method since it is possible to ensure computational efficiency for contact detection and force calculations [3-5]. As the contact between two spheres is different from that between two cylinders, the latter should be calculated in order to consider the real contact. The authors have proposed a contact model on the basis of each contact pattern for rod-like particles [6]. It was found that the numerical approach is effective for estimating the vibratory conveyance of acrylic resin cylinders. More studies are required in order to apply

the numerical approach to many engineering problems related to the motion of rod-like particles.

In this work, an inclined chute flow of rod-like particles is investigated both experimentally and analytically. The behavior of the particles is solved by the DEM. The rod-like particle model consists of a cylinder, capped at both ends by hemispheres whose radii are the same as the radius of the cylinder. The rod-like particles have three translational degrees of freedom, their rotational motion being described through quaternions, and the interparticle contact is described by a force that accounts for the elastic and dissipative interactions. The contact patterns for rod-like particles are divided into six types. In the experiment, brass and acrylic resin cylinders of uniform size were used. The validity of the theory was confirmed by comparing the experimental and analytical results. In addition, the effect of the particle material on the flow pattern was examined.

2 COMPUTATIONAL MODEL

Figure 1 shows the computational model. In this paper, the rod-like particle model consists of a cylinder with length L and two hemispheres with the same radius r. The translational motion of particle i is governed by Newton's second law of motion:

$$\sum_{j=1}^{N_c} \boldsymbol{F}_{ij} = m\ddot{\boldsymbol{r}}_i \,, \tag{1}$$

where N_c is the number of particles in contact with particle i, $\boldsymbol{F}_{ij}$ is the force exerted by particle j on particle i, and m is the particle mass.

Euler's rotational equations of motion for particle i become

$$\begin{aligned} I_X\dot{\omega}_i^X - (I_Y - I_Z)\omega_i^Y\omega_i^Z &= T_i^X \\ I_Y\dot{\omega}_i^Y - (I_Z - I_X)\omega_i^Z\omega_i^X &= T_i^Y \\ I_Z\dot{\omega}_i^Z - (I_X - I_Y)\omega_i^X\omega_i^Y &= T_i^Z \end{aligned} \,, \tag{2}$$

where I is the principal moment of inertia, ω is the angular velocity, and T is the torque acting on particle i.

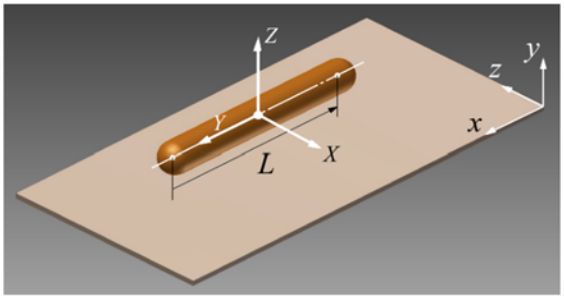

Figure 1: Rod-like particle model

3 PHYSICAL CONTACT MODEL

The contact patterns for rod-like particles are divided into six types. There are two patterns of contact between a rod-like particle and a wall, as shown in Figure 2. In the case of

interparticle contact, there are four contact patterns, as shown in Figure 3. The contact forces are determined by Hertzian contact theory.

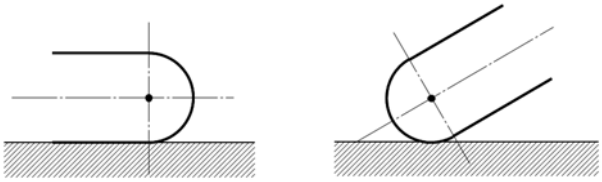

(a) Cylindrical contact (b) Hemispherical contact

Figure 2: A particle in contact with a wall

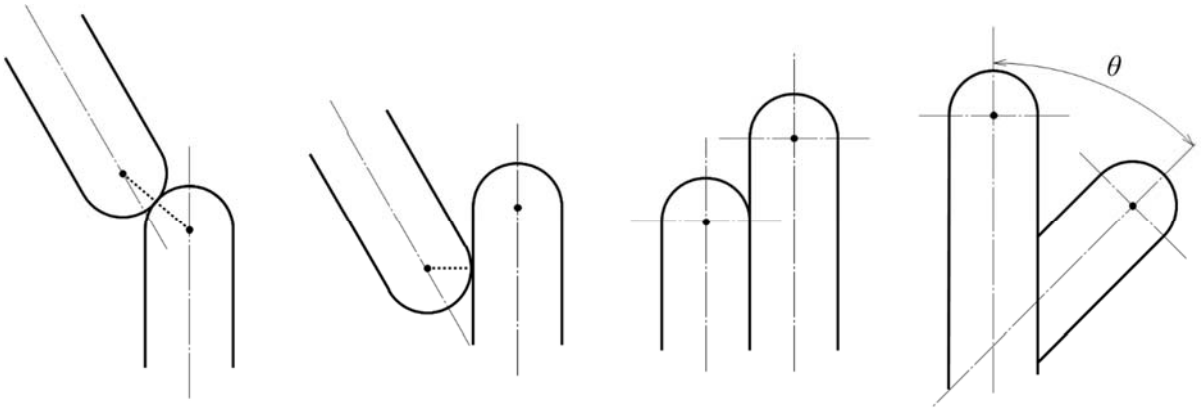

(a) Contact between two hemispheres (b) Contact between a hemisphere and a cylinder (c) Parallel Contact between two cylinders (d) Nonparallel contact between two cylinders

Figure 3: Interparticle contact

3.1 Cylinder in contact with wall

Figure 2(a) shows the contact between a cylindrical part and a wall. If a cylinder and a wall are pressed into contact with force P, then the half-width w of the contact area is expressed as

$$w = \sqrt{\frac{4rP}{\pi L}\left(\frac{1-{\nu_p}^2}{E_p}+\frac{1-{\nu_w}^2}{E_w}\right)}. \tag{3}$$

The deformation δ_n is given by

$$\delta_n = \frac{P}{\pi L}\left(\frac{1-{\nu_p}^2}{E_p}+\frac{1-{\nu_w}^2}{E_w}\right)\left(1.8864 + ln\frac{L}{2w}\right), \tag{4}$$

where E is the modulus of elasticity and ν is Poisson's ratio [7]. Subscripts p and w denote a particle and a wall, respectively.

Figure 4 shows the relationship between the deformation δ_n and P in the case of contact between a cylinder and a wall. The conditions used in the calculation are given in Table 1. The length L and radius r of the cylinder are 117.04mm and 1.98mm, respectively. In this figure, P

is proportional to δ_n and the coefficient of proportionality can then be determined from the slope k.

Table 1: Values of parameters

Modulus of elasticity E_p (GPa)	Acrylic resin	3.14
Modulus of elasticity E_p (GPa)	Brass	103
Modulus of elasticity E_w (GPa)	ABS	2.65
Poisson's ratio ν_p	Acrylic resin	0.35
Poisson's ratio ν_p	Brass	0.35
Poisson's ratio ν_w	ABS	0.35

Supposing that the normal component F_n of the contact force acting on the particles is given by the sum of the damping force and the elastic force, F_n is given by

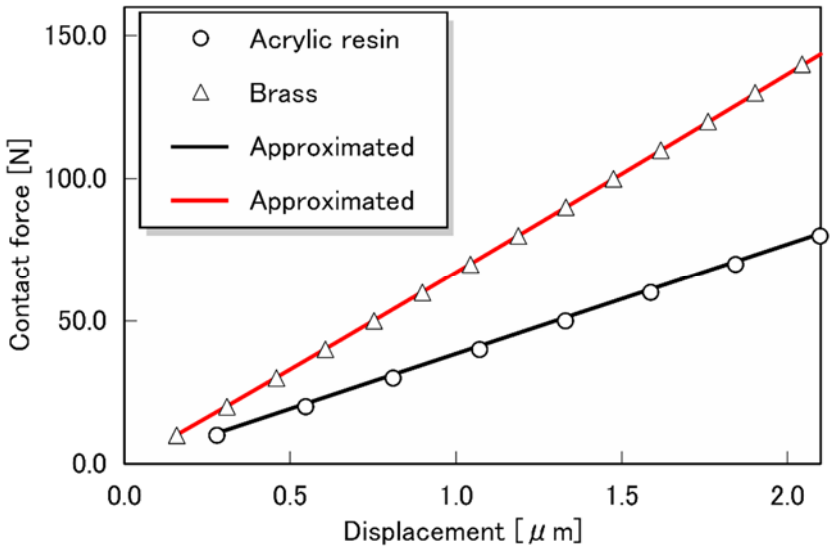

Figure 4: Contact force vs. deformation in the case of contact between a cylinder and a wall

$$F_n = k\delta_n + c\dot{\delta}_n \,, \tag{5}$$

where the damping coefficient c [7] is

$$c = \frac{2\sqrt{mk}}{\sqrt{1 + (-\pi/lne)^2}}. \tag{6}$$

The tangential force F_t is given by

$$F_t = -\frac{\mu F_n \dot{\delta}_t}{|\dot{\delta}_t|} \,, \tag{7}$$

where $\dot{\delta}_t$ is the tangential velocity and μ is the coefficient of friction between the particle and the wall.

3.2 Hemispherical part in contact with wall

Figure 2(b) shows the contact between a hemispherical part and a wall. Supposing that the contact is the same as that between a sphere and a wall, the normal component F_n of the contact force is given by

$$F_n = k{\delta_n}^{3/2} + \alpha\sqrt{mk}{\delta_n}^{1/4}\dot{\delta_n}\,. \tag{8}$$

The spring constant k is given by

$$k = \frac{4\sqrt{r}}{3}\cdot\frac{E_p E_w}{(1-{\nu_p}^2)E_w + (1-{\nu_w}^2)E_p}. \tag{9}$$

The damping constant α is determined from the coefficient of restitution [8].

3.3 Contact between hemispherical parts

Figure 3(a) shows the contact between two hemispherical parts. Supposing that the contact is the same as that between two spheres, the normal component F_n of the contact force is also given by Eq. (8). The spring constant k is given by

$$k = \frac{\sqrt{2r}E_p}{3(1-{\nu_p}^2)}. \tag{10}$$

3.4 Hemispherical part in contact with cylindrical part

Figure 3(b) shows the contact between a hemispherical part and a cylindrical part. In the case of contact, the normal component F_n of the contact force is also given by Eq. (8). The spring constant k [6] is given by

$$k = 0.974^{(-3/2)}\sqrt{\frac{8r}{27}}\cdot\frac{E_p}{1-{\nu_p}^2}. \tag{11}$$

3.5 Contact between two cylinders with parallel axes

Figure 3(c) shows the contact between two parallel cylindrical parts. If two cylinders are pressed together by force P, then the half-width w of the contact area is expressed as

$$w = \sqrt{\frac{4rP}{\pi L E_p}(1-{\nu_p}^2)}\,. \tag{12}$$

The deformation δ_n is given by

$$\delta_n = \frac{2P}{\pi L}\left(\frac{1-{\nu_p}^2}{E_p}\right)\left(1.8864 + ln\frac{L}{2w}\right). \tag{13}$$

Figure 5 shows the relationship between the deformation δ_n and the force P in the case of contact between two parallel cylinders. The conditions used in the calculation are given in Table 1. The length L and radius r of the cylinder are 117.04mm and 1.98mm, respectively. In this figure, $P$is exactly proportional to δ_n Therefore, in the case of contact, the normal component F_n of the contact force is also given by Eq. (5).

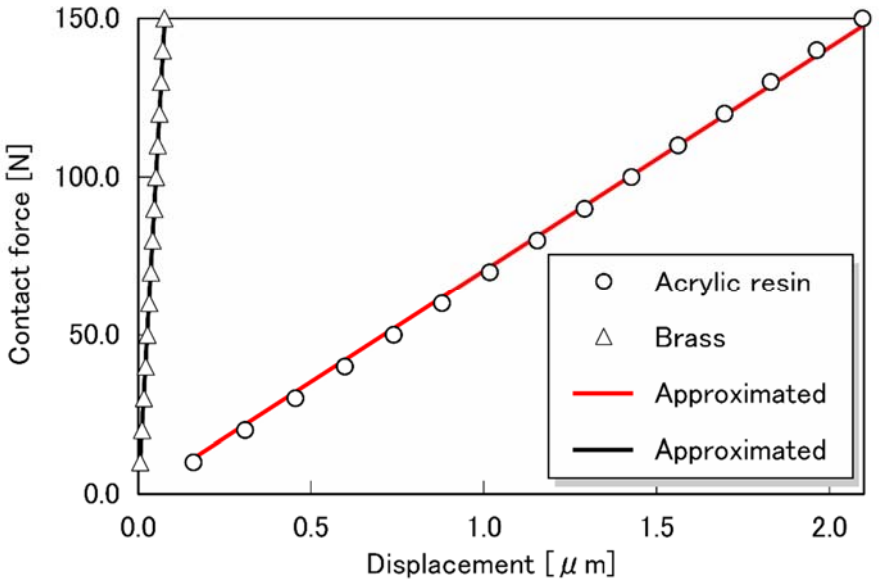

Figure 5: Contact force vs. deformation in the case of contact between two parallel cylinders

3.6 Contact between two cylinders with inclined axes

Figure 3(d) shows the contact between cylinders with inclined axes. In the case of contact, the normal component F_n of the contact force is also given by Eq. (8). The spring constant k [9] is given by

$$k = \frac{2}{3}\sqrt{r}\left(\frac{2K}{\pi\varepsilon}\right)^{(-3/2)} \cdot \frac{E_p}{1-{\nu_p}^2}, \tag{14}$$

where K and ε are

$$K = \int_0^{\pi/2} \frac{d\phi}{\sqrt{1-a^2 sin^2\phi}}, \tag{15}$$

$$\varepsilon = \sqrt[3]{\frac{1}{1-a^2} \cdot \frac{2S}{\pi}}. \tag{16}$$

In Eq. (16), S is given by

$$S = \int_0^{\pi/2} \sqrt{1-a^2 sin^2\phi}\, d\phi\,, \tag{17}$$

where a is the modulus of the elliptic integral. The contact angle θ is given by

$$\theta = cos^{-1}(2b^2 - 1)/2\,, \tag{18}$$

where b is given by

$$b = \frac{(2-a^2)S - 2(1-a^2)K}{a^2 S}. \tag{19}$$

Figure 6 shows the relationship between the spring constant k and the contact angle θ for the contact between cylinders with inclined axes.

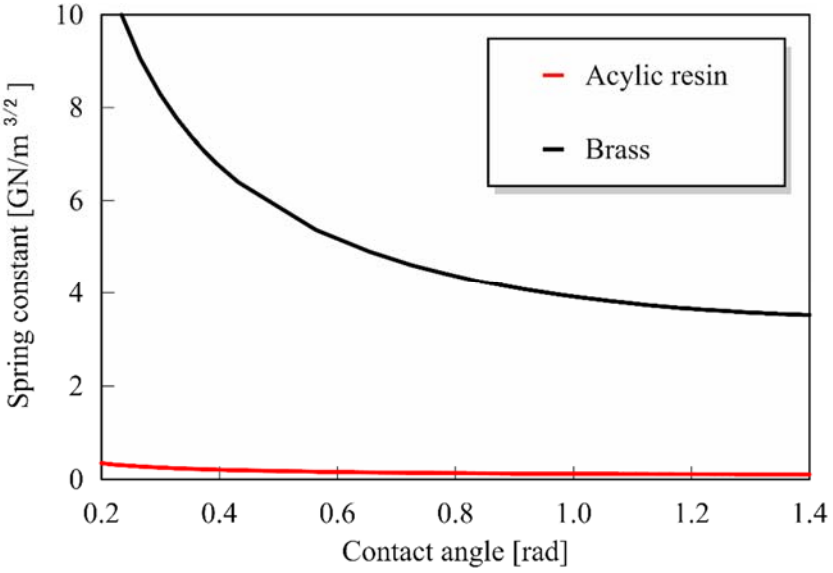

Figure 6: Spring contact vs. contact angle

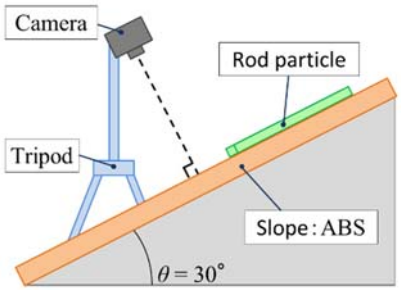

Figure 7: Experimental apparatus

4 EXPERIMENTS AND NUMERICAL APPROACH

Experiments were carried out to verify the validity of the numerical approach. In this study, the simulation code was developed using C++ language and OpenGL.

Figure 7 shows the experimental apparatus. The inclined chute was made of ABS and the inclination angle was 30°. The behavior of the particles was observed with a high speed camera (Casio Exlim EX-100) at 240fps and their movements were obtained with an image processing system. Brass and acrylic resin cylinders of uniform size were used.

Figure 8 shows the initial positions of six rod-like particles on the inclined chute. To examine the effect of interparticle contact, two particles were fixed firmly on the chute.

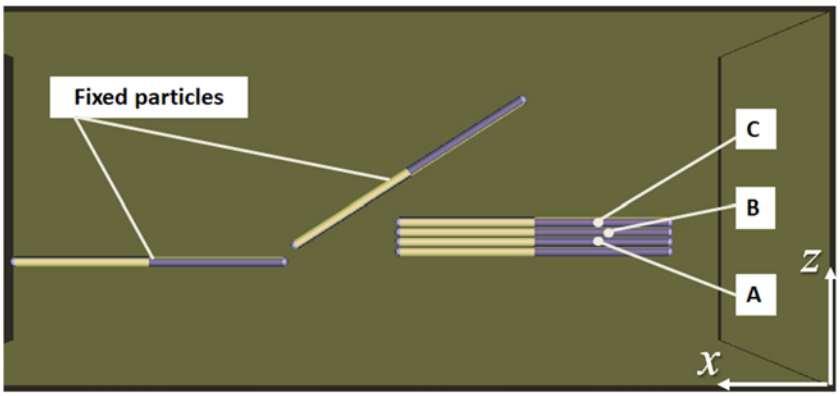

Figure 8: Initial positions of rod-like particles

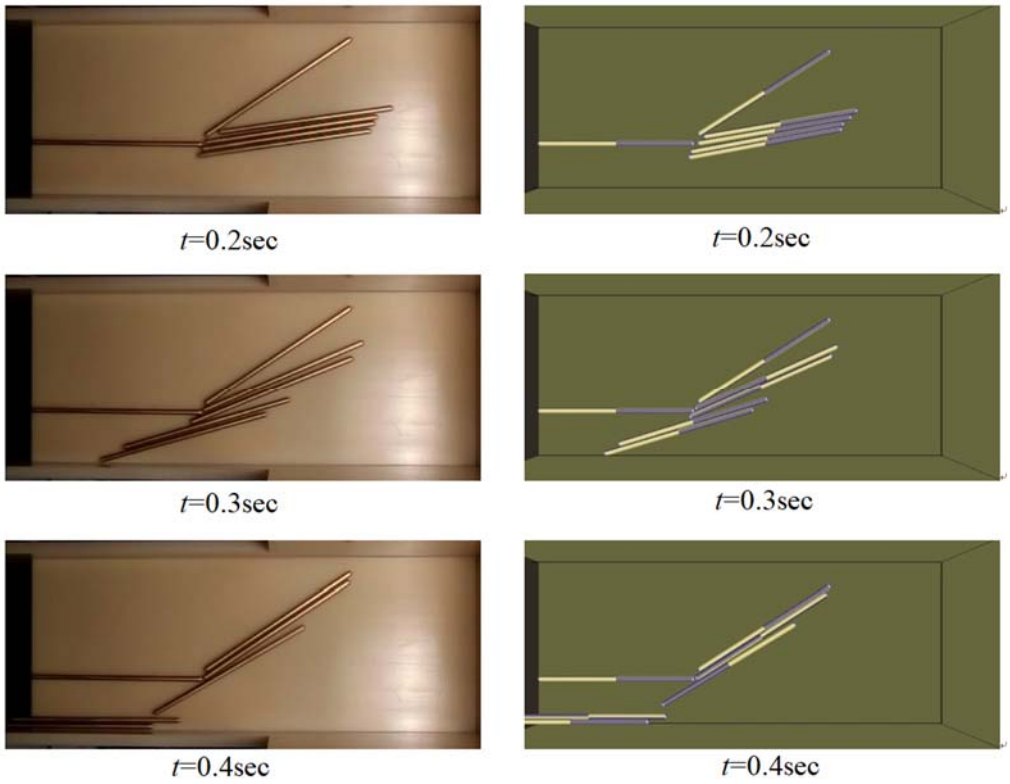

(a) Experimental results (b) Calculated results

Figure 9: Behavior of Brass particles

5 RESULTS AND DISCUSSION

Figures 9(a) and 9(b), respectively, show photographs of the experimental results and computer graphics created using the calculated results under the same conditions. It is found that the typical features of flow patterns of brass particles observed in the experimental results are well reproduced in the calculated results.

Figures 10(a) and 10(b) show the effects of the initial position of the brass particles and the

particle material on the time history of the movement of the particles along the *x*-axis, respectively. These figures also show the analytical and calculated results. This experiment was carried out three times. It was found that the effect of the initial position on the movement is greater than that of the particle material. It was also observed that the calculated results are in reasonably good agreement with the experimental results. Therefore, the numerical approach is effective for estimating the dynamical behavior of rod-like particles.

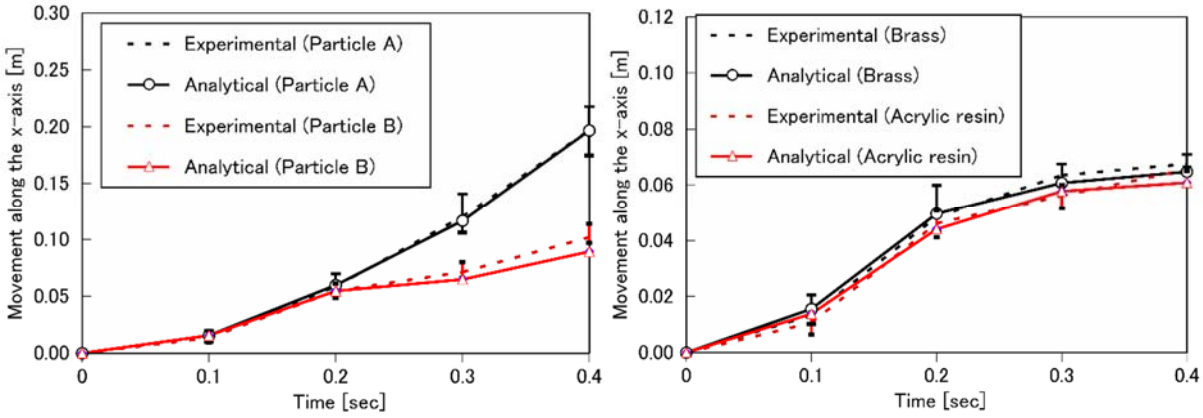

(a) Brass particles A and B (b) Brass and acrylic resin (particle C)

Figure 10: Time histories of the movement along the *x*-axis

6 CONCLUSIONS

An inclined chute flow has been modeled using the DEM for rod-like particles in order to understand the effect of the particle shape on such flows. The contact patterns for rod-like particles was classified into six types. The behavior of the rod-like particles was observed with a high speed camera and their movements were obtained with an image processing system. From the time histories of the movements for rod-like particles, it was found that the calculated results agree with the experimental results. Therefore, the numerical approach in this study is effective for addressing the engineering problems of rod-like particles.

REFERENCES

[1] Haeri, S., Wang, Y., Ghita, O. and Sun, J. Discrete element simulation and experimental study of powder spreading process in additive manufacturing, *Powder Technology*(2016) **306**: 45-54.

[2] Markauskas, D and Kacianauskas, R. Investigation of rice grain flow by multi-shpere particle model with rolling resistance, *Granular Matter* (2011)**13**: 143-148.

[3] Deng, X. L. and Dave, R. N. Dynamic simulation of particle packing influenced by size, aspect ratio and surface energy, *Granular Matter*(2013)**15**: 401-415.

[4] Marigo, M and Stitt, E. H. Discrete element method (DEM) for industrial applications: Comments on calibration and validation for the modelling of cylindrical pellets, *KONA Powder and Particle Journal* No.32 (2015): 236-252.

[5] Pournin, L., Weber, M., Tsukahara, M., Ferrez, J. A., Ramaioli, M. and Liebling, T. M. Three-dimensional distinct element simulation of spherocylinder crystallization, *Granular Matter* (2005) **7**: 119–126.
[6] Kidokoro, T., Arai, R. and Saeki, M. Investigation of dynamics simulation of granular particles using spherocylinder model, *Granular Matter* (2015) **17**: 743–751.
[7] Saeki, M., Minagawa, T. and Takano, E. Study on vibratory conveyance of granular materials JSME *International Journal C* (1998)**41**. No.4:704-709.
[8] Tsuji, Y., Tanaka, T. and Ishida, T. Lagrangian numerical simulation of plug flow of cohesionless particles in a horizontal pipe, *Powder Technology* (1992)**71**: 239-250.
[9] Okamoto, J., Nakayama, K., and Sato, M. *Introduction to tribology*, Saiwai Shobo (1990)